Asian Journal of Physics
Vol. 32, Nos 1 & 2 (2023) A1-A10
Available on: www.asianjournalofphysics.com

ap

Resonant Raman scattering in semiconductor nanostructures and thin films

Andrés Cantarero and Carlos Rodríguez-Fernández

Molecular Science Institute, University of Valencia, PO Box 22085, 46071 Valencia, Spain

Raman spectroscopy is a versatile technique which provides valuable information of many physical properties of solid: crystals and nanostructures from its characteristic phonon spectrum. Magnetic phase transitions are observed through the change of the phonon spectrum or the behaviour of particular phonon modes, surface states or interfaces can be studied through the appearance of new phonon modes, the electronic structure of solids can be analysed by means of resonant Raman scattering, the stress can be obtained by analysing the shift of non-polar phonons and the knowledge of the phonon deformation potentials. These are a few examples of the power of this standout technique. Micro-Raman spectroscopy allows the successful analysis of tiny amounts of samples, single quantum dots, quantum wires or two-dimensional materials. In this paper, after a brief theoretical introduction, we will give some examples of the use of resonant Raman scattering in the study of semiconductor nanostructures and thin films.

Keywords: Raman spectroscopy, Electron-phonon interaction, Semiconductor nanostructures.

1 Introduction

Raman scattering or inelastic light scattering is the scattering of the light by any kind of quasiparticles in a solid. In semiconductors, a Raman experiment refers usually to the scattering of the light by phonons. In semiconductor nanostructures like superlattices (SLs), acoustic phonons are folded due to the larger lattice parameter of the SL giving rise to the existence of mini-Brillouin Zones (mBZ). Optical phonons are confined in the mBZ [1]. There is a large variety of quantum dots and quantum wires; the description of the phonons in these systems being out of the scope of the present review, but in general, in most of the nanostructures, optical phonons are not confined (it is not the case of a SL). The reason is that while the electron confinement is produced when the dimensions of the nanostructures are below 10 nm, in the case of phonons, there is no confinement above 2-3 nm [2].

Although Raman scattering by phonons is usually discussed in terms of one phonon processes, in the Raman spectra we can usually observe the phonon density of states (DOS), more precisely the two-phonon DOS. The reason is that, while in the case of one-phonon processes, we have the wave number conservation, $\boldsymbol{q} = \boldsymbol{k}_l - \boldsymbol{k}_s \approx \mathbf{0}$, $\boldsymbol{q}$ being the phonon wave vector, while $\boldsymbol{k}_l$ and $\boldsymbol{k}_s$ are the wave number of the laser/scattered light; in the case of two-phonons the wave number conservation results in $\boldsymbol{q}_1 + \boldsymbol{q}_2 \approx 0$, the phonon wave vectors can be inside the BZ provided the sum of both wave vectors is nearly zero. The two phonon DOS appears usually as a background in a Raman spectrum, and it is usually observable out of resonance, but higher orders in the DOS are usually very weak and not observed. When the laser light is of the order of an electronic transition in the semiconductor, there is an enhancement of the Raman signal due to resonance effects and usually DOS is a very small background and not observed. On the other hand, if the quality of the sample is very poor with a lot of defects, the translational symmetry of the crystal can be lost. In that case, the one phonon DOS can also appear in a Raman spectrum together with weak phonon modes originated in the crystalline or polycrystalline regions [3].

**Based on the lecture delivered at ICOPVS2022, Dec 13-17,2022, Indore, India.*

Corresponding author
e mail: Andres.Cantarero@uv.es (Andrés Cantarero)

The purpose of this study is to discuss a selected set of experiments which have allowed the observation of some peculiarities in nanostructures or thin films by using the resonant Raman scattering technique. After a theoretical background, we will discuss the tailoring of the magnetism in STO/BTO SLs, the quantification of Te clusters in Bi_2Te_3 nanowires, the observation of silent modes due to the isotopic composition of Ga and N in GaN ultra-thin nanowires, the power of Raman scattering in comparison with x-ray diffraction (XRD) in a few layers Bi films and the distinction between the photoluminescence and Raman in ZnTe films, together with the appearance of multi-phonon processes due to Fröhlich electron-phonon interaction.

2 Theoretical Background

In an infrared experiment, the electric field of the light interacts directly with the optical vibrations of the crystal since the phonon frequency (energy) is of the same order of that of the light. But in the case of Raman scattering the light couples the phonons via the electronic states, which participate in the process as virtual states. When the energy of the light is close to the fundamental gap of a semiconductor or a semiconductor nanostructure, the virtual electronic states become excitons. In Fig 1 the parabolic bands of a standard semiconductor are shown in the exciton representation, where we display the band structure as a function of the centre of mass wave vector **K** : The figure shows the bound exciton states (n = 1, 2,…) and the continuous or correlated electron-hole pairs states with $k = k_e - k_h$ (they corresponds to the shadow region above the parabolic bands). The absorption of a photon can be considered a vertical transition since the wave number of the light (in the green region of the spectrum) is $k \approx 1.25 \times 10^5$ cm^{-1}, while the size of the BZ is 1000 times larger. Thus, the only electronic states excited by the light in a first order Raman process (one phonon) correspond to $K = 0$

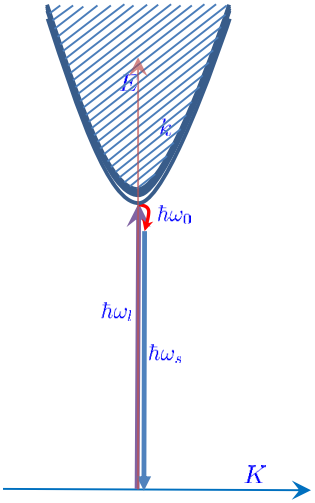

Fig 1. A semiconductor band structure in the exciton representation.

Figure 2 shows the most important Feynman diagrams of the Raman process. In the upper part, a photon with energy $\hbar\omega_i$ creates an electron-hole pair (an exciton) and the electron emits a phonon of energy $\hbar\omega_0$ (it could also absorb a phonon) and recombines again with the hole, emitting the scattered photon of energy $\hbar\omega_S$. In the lower part, the hole emits the phonon. The photon lines are the wavy lines, the electron-hole pairs (excitons) the dashed lines while the phonon is depicted with a solid line. The Raman intensity is usually given in terms of the scattering efficiency per unit solid angle, which is defined as [4]

$$\frac{dS}{d\Omega} = \frac{\omega_s^3\,\omega_l}{c^4}\,\frac{\hbar}{2\upsilon_d\mu\omega_0}\,\frac{n_s}{n_l}\,|\,e_l\,\mathcal{R}\,e_s\,|[N(\omega_0)+1]$$

c being the speed of light, υ_c the volume of the unit cell, μ the exciton reduced mass and n_s and n_l the refractive index of the laser and scattered photon, respectively. $N(\omega_0)$ is the phonon population and $\mathcal{R}$ is the Raman tensor, which for the E_1 phonon of the wurtzite structure, for instance, is:

$$\mathcal{R} = E_1(x) = \begin{pmatrix} 0 & 0 & c \\ 0 & 0 & 0 \\ c & 0 & 0 \end{pmatrix}$$

and e_l and e_s the polarization of the incoming and outgoing photons. The Raman tensor is written in terms of the Raman polarizability c, given by

$$\mathrm{c} \propto \sum_{I,\,F} \left| \sum_{\mu,\mu'} \frac{\langle I|H_{er}|\mu\rangle\langle\mu|H_{ep}|\mu'\rangle\,\langle\mu'|H_{er}|F\rangle}{(E_\mu - \hbar\omega_l + i\gamma_\mu)\,(E_{\mu'} - \hbar\omega_s + i\gamma_{\mu'})} \right.$$

μ and μ' are the intermediate excitonic states, I and F the initial and final states, which may correspond to the ground state, since the only real quasiparticles in a Raman process are the photons and the phonon. Since a Raman process is given in terms of second order perturbation theory, the Raman polarizability contains two denominators. When the energy of the laser coincides with an excitonic state we say that we are in incoming resonance. It is the case shown in Fig 1, where the laser energy coincides with the n =1 exciton. If the scattered photon coincides with an excitonic state, we are in outgoing resonance. In super lattices or under uniaxial stress, both denominators can be nearly zero and we have a double resonance [5]. In two-phonon resonance Raman scattering we can have triple resonance [6].

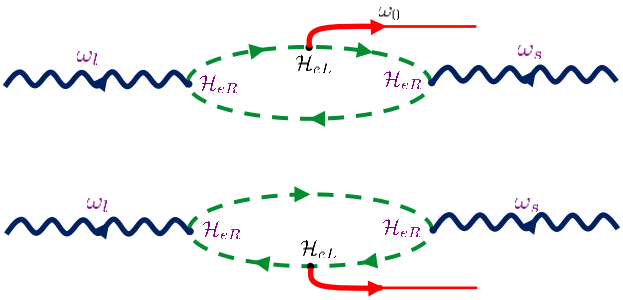

Fig 2. Feynman diagrams corresponding to the two most important processes near resonance.

For optical phonons with nearly zero wave number, i. e. in the long wavelength limit ($\lambda >> a$, a being the lattice parameter), the electron-phonon Hamiltonian has two contributions, one of short range, called deformation potential interaction, and other a long-range interaction called Fröhlich interaction. The short-range contribution is produced in the surrounding of a unit cell, and it is tightly related with the elastic tensor of the solid. The electron wave function in a solid (Bloch function) is the product of a periodic function times a plane wave. The deformation potential acts on the periodic part of the wave function, either that of the electron (the electron emits or absorbs a phonon) or the hole (the hole emits or absorbs the phonon). The long-range contribution is practically constant along several unit cells and it is basically due to the potential set up by the polarization of the lattice emerging when the phonons vibrate. This is called Fröhlich interaction. Since, it is a long-range interaction the corresponding Raman tensor is diagonal, it is not related to the local structure of the crystal.

The Raman selection rules are related to the crystal symmetry and thus to the deformation potential interaction. In resonance, where Fröhlich interaction dominates, the selection rules do not play any role, since the Fröhlich Hamiltonian is diagonal (phonons are observed in parallel polarisations). But, since Fröhlich interaction is the electrostatic interaction between the phonons and the electrons, it enhances only the polar optical phonons. In covalent crystals there is no Fröhlich interaction.

Next, we will give a few examples of applications of resonant Raman spectroscopy to extract information on different kinds of nanostructures and thin films.

3 Nanoscale ferroelectricity in BTO/STO superlattices

Ferroelectricity can be manipulated in the nanoscale, as we have shown some years ago [7]. While the bulk value of the phase transition temperature T_C in barium titanate (BTO) is 403 K, by fabricating a $SrTiO_3/BaTiO_3$ super lattice, we were able to show that T_C can be engineered from 250 K to 235 K, below and above the bulk value, respectively. Strontium titanate (STO) has an optical band gap of 3.27 eV [8] while that of barium titanate (BTO) is 3.47 eV [9], both in the ultraviolet region of the spectrum. The Raman response of a STO/BTO superlattice (SL) using the typical 514.53 nm line of an Ar ion laser can be observed in Fig 3 (blue line) in comparison with a bare substrate (black line) [7]. There is basically no difference between the Raman spectra of the substrate and the superlattice, the only signal observed is coming from the STO substrate. The problem is the small amount of material, which produces a very weak Raman signal. It was nearly impossible to extract some useful data from a film below 100 nm. But, when the Raman spectrum is recorded with the 351.1 nm line of an Ar laser, i.e. in resonance with the electronic structure of the compound, we observed the whole structure of the SL, starting from the folded acoustic phonons of the superlattice.

The experiment was performed in a T64000 triple spectrometer in additive mode with an open electrode CCD. In the triple spectrometer the stray light was strongly reduced, and the resolution was improved. The indices n and m in the BTO_n/STO_n SLs refer to the number of unit cells in the growth direction. In Fig 3, we observe several confined modes of the SL in red, the mode around 180 cm^{-1} close to the TO_2 peak of the electric-field induced Raman mode of STO which is originated in the SL since the phonons of bulk STO are Raman forbidden. The mode around 290 cm^{-1} is also close to the A_1 mode and corresponds to the tetragonal phase of BTO, thus it has been assigned due to the BTO layer. The LO_3 and TO_4 involve both BTO and STO layers, i. e. confined modes of the superlattice. When BTO becomes paraelectric, the induced electric field on the STO layer disappears and thus the corresponding phonon mode disappears. By monitoring the phonon mode as a function of temperature, we can accurately predict T_C.

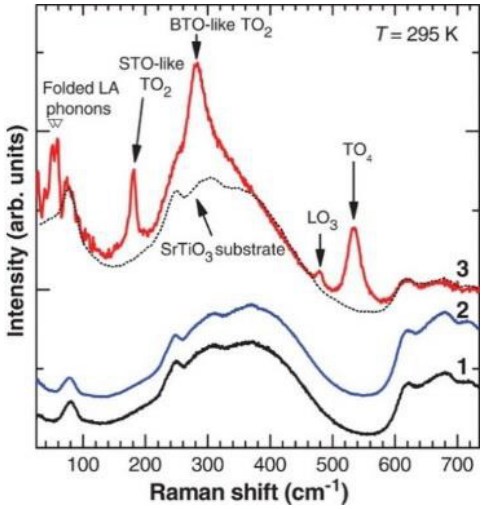

Fig 3. Raman spectra of (1) a STO substrate, (2) a BTO_5/STO_5 SL and (3) the same SL measured in the UV [7]. Reprinted with permission from AAAS.

In Fig 4, the Curie temperatures for different superlattices have been plotted as a function of the number of BTO unit cells in the SL for two different superlattices with $m = 4$ and 13. We can realize that even

in the case n =1 (0.43 nm), the superlattice is ferroelectric. This shows the power of the ferroelectricity at the nanoscale.

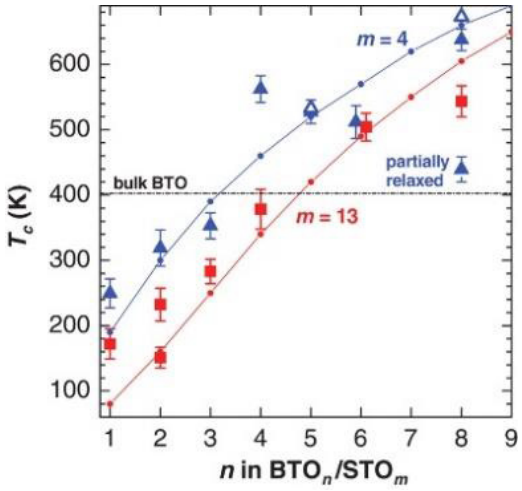

Fig 4. T_C as a function of the number of BTO layers for m = 4, 13 [7]. Reprinted with permission from AAAS.

4 Resonant Raman scattering in bismuth telluride nanowires

In the framework of a project on thermoelectricity, we were studying the role of diameter in Bi_2Te_3 nanowires for their thermoelectric properties. A careful analysis of the Raman spectra of the different nanowires was done. In this way, we found that the best quality nanowires were the thinnest ones. Inspecting the nanowires with RRS, we realized that the worst quality nanowires had only three peaks at different frequencies, thus they do not belong to Bi_2Te_3.

Looking at the literature we found several papers claiming that these modes were the fingerprint of the existence of a quintuple layer of Bi_2Te_3. The modes were assigned as IR active, which became Raman active due to the lack of translational symmetry [10]. In other works published by Balandin's group, they assigned the new modes to one or two IR active modes. The most cited papers of the group on the subject have nowadays 385 and 225 citations. Thus, more than 600 papers were using the wrong argument that these modes belonged to Bi_2Te_3 and were IR modes. Supporting our data with a careful analysis by transmission electron microscopy (TEM) and comparing the Raman spectrum with a pure Te sample it became evident that the modes were originated by Te clusters. This was confirmed by TEM measurements, and we discovered that the nanowires with smaller radius were the most stoichiometric, while the thicker nanowires presented Te clusters. The detailed analysis of the TEM in conjunction with the Raman data have been published in Nanotechnology [11]. In Fig 5 we show the Raman spectra of nanowires with different diameters, they have been labelled taking into account the Te-content. The excess of Te-content in the compound can be quantified by a parameter δ extracted from the chemical formula $Bi_2Ti_{3(1+\delta)}$. In this way, δ = 0, represents the stoichiometric expression. The value of δ has been obtained from HRTEM-EDX measurements. In the figure, the upper spectrum corresponds to a nanowire keeping the stoichiometry (30 nm diameter), and the following three spectra to nanowires with different stoichiometry. The last spectrum corresponds to a Te thin film, where we can observe the E_1, A_1 and E_2 modes of Te. The position of these phonons has been taken into account in the fitting shown in the upper spectra. As it is clearly seen, the contribution of the Te phonons in the spectra increases with δ.

5 Observation of forbidden modes in Raman scattering

In this section, we will discuss the appearance of a silent mode in resonant Raman scattering and the reason why this forbidden mode appears. Gallium nitride (GaN) has 9 optical modes: a one dimensional A_1 mode and the two dimensional E_1 mode are polar (observed in Raman and IR), the two E_2 modes are non -polar (observed only in Raman) and finally the two B_1 modes are silent (observed neither in Raman nor in IR). As it is well known, polar modes are much stronger under resonance due to the Fröhlich contribution, thus we can expect the appearence of the A_1 and E_1 modes under resonance.

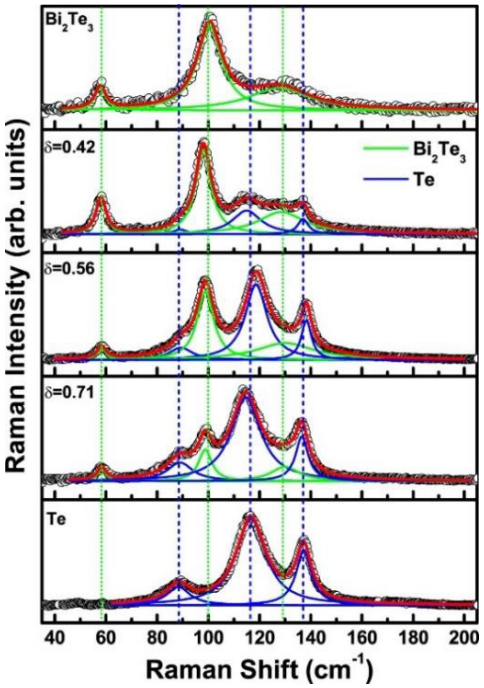

Fig 5. Room-temperature Raman-scattering spectra of Bi_2Te_3 nanowires for samples with different Te content, indicated by δ [11]. Reprinted with permission from IOP.

We have measured RRS in a sample of very narrow GaN nanowires grown on a silicon substrate using several laser lines from the red region of the spectrum to the ultraviolet (the gap of GaN is of the order of 3.4 eV). The Raman spectra are displayed in Fig 6. Since the sample was grown on Si, the main observation is the Si peak around 520 cm^{-1}, while the E_{2h} mode of GaN appears as a shoulder of the Si peak. Using the green line, where Si shows RRS, the E_2 mode also appears, but the main signal is still the LO peak of Si, which has been multiplied by a factor in order to observe the density of states of Si, in particular the peak around the 2TA(X) is clearly observed around 300 cm^{-1}. Exciting the samples with a blue laser of 488 nm, which is in resonance with electronic transitions in GaN, the Si peak decreases, since silicon is becoming out of resonance, and we continue observing the E_2 mode of GaN. Finally, when the sample was excited with the 325 nm line of a He-Cd laser, the Si peak still appears, although very weak (the direct gap of Si is around 3.85 eV), but it absorbs most of the light and only a small volume contributes to the Raman scattering and two additional modes appear, the A_1(LO), located at 734.1 cm^{-1} and the B_{1l} mode, at 320.4 cm^{-1}. The frequency of the B_{1l} mode coincides with DFT calculations, and also with the phonon dispersion measured by inelastic x-ray scattering [13]. The reason why the B_{1l} appears is clearly due to the polar character of the mode and the presence of Fröhlich interaction. But, how the B_{1l} mode becomes

a polar mode while the B_{1h} does not? Both are silent modes! The explanation can be found in the isotopic compositions of both modes. The B_{1h} mode corresponds basically to the movement of N atoms, which are 99% isotopically pure and thus it does not present polarity, while the B_{1l} mode corresponds mainly to the movement of Ga atoms, which have a nearly 40/60 composition of ^{69}Ga and ^{71}Ga, respectively. Since the phonon frequency is inversely proportional to the square root of the mass, there is a slightly different frequency (which depends on the square root of the mass) giving rise to a beating and a polar contribution which is present in the B_{1l}, but not in the B_{1h}. A more detailed explanation has been given in the original paper [12].

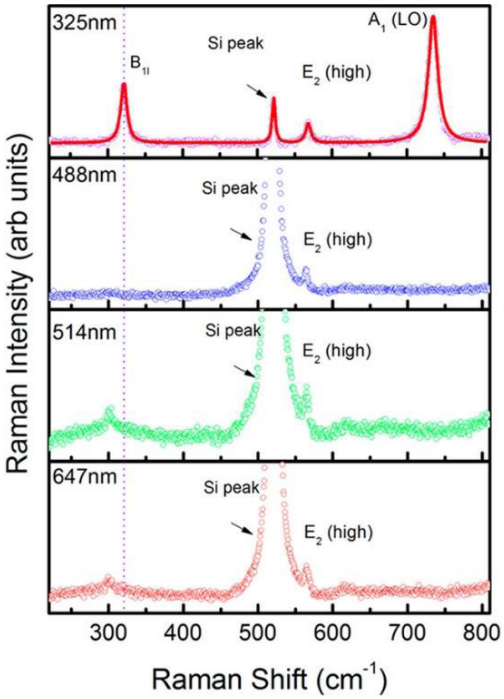

Fig 6. Raman spectra of GaN nanowires covering the range of interest. From top to bottom we show the spectra obtained with the laser line excitations 325, 488, 514, and 647 nm, respectively. Reprinted with permission from [12]. Copyright 2021, American Chemical Society.

6 Crystallinity of Bi films on an amorphous substrate measured by RRS

Bulk bismuth is a semimetal with a small overlap of the bands giving a very slow carrier density, typical of a semiconductor. It shows exotic properties when growing below 20 nm. In particular, it has been shown that a Bi-bilayer is a 2D material presenting quantum spin Hall effect [14]. Since suspended bilayers are not stable, they need to be grown on a suitable substrate for further studies and applications. Although a few Bi monolayers (ML) have been successfully grown on crystalline substrates, it is more convenient to grow them on an amorphous substrate in order to characterize the Bi layers. In this way, in an x-ray experiment, the only signal producing Bragg peaks will be that coming from the Bi, since the amorphous substrate only produces a background. Also, in a Raman experiment an amorphous substrate gives only the density of states. Different Bi films, from 40 to 5 nm, were grown on a SiO_2 amorphous substrate [15] and have been characterized by x-ray diffraction (XRD). The XRD experiments show the (111) and (222) peaks at $\theta = 22.5$ and 46 degrees, approximately, but only in the 40 and 20 nm samples. The other two samples (10 and 5 nm) were amorphous for XRD. Fortunately, bismuth shows an acceptable resonant Raman signal using

the 647 nm line of a Kr-Ar laser. In Fig 7, we show the RRS spectra of the several rhombohedral Bi layers from 40 to 5 nm. The RRS spectra clearly show that all the samples, even the thinner one, are crystalline. Thus, by means of RRS we were able to show that even the 5 nm layer was crystalline when grown in an amorphous substrate. Thus, resonant Raman scattering is able to provide more information than XRD in many cases and this is a typical example.

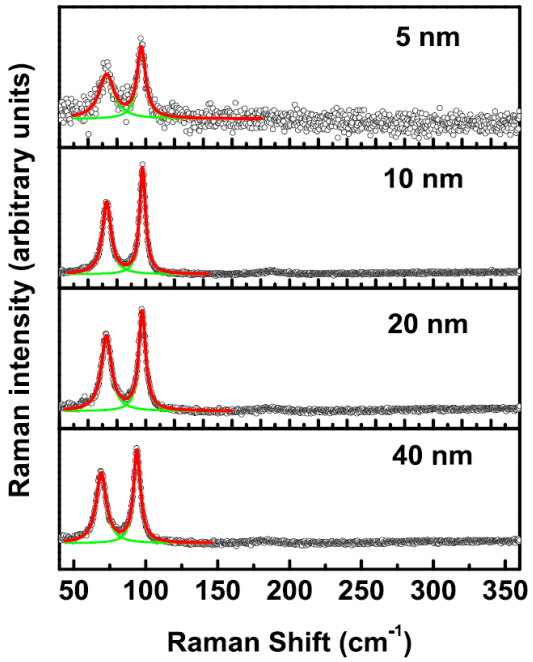

Fig 7. Room-temperature Raman-scattering spectra of Bi thin films with a thickness of 5, 10, 20 and 40 nm (from the upper to lower panel). From [15]. Reprinted with permission.

7 Multi-phonon RRS in ZnTe thin layers on GaAs

Another example of RRS is that of ZnTe [15]. Zinc telluride is a 12-16 semiconductor with an electronic gap around 2.4 eV at low temperatures. A ZnTe thin film was grown on a GaAs substrate by molecular beam epitaxy method. In Fig 8, we show the photoluminescence (PL) spectra, measured with two different excitation energies, 2.4972 eV (496.5 nm) and 2.5464 eV (486.9 nm). The vertical dashed lines divide the whole region into three with different scales, giving more detail in the last region at the right, where we have more structure. The upper plot refers to the highest energy excitation, while the lower plot corresponds to the lower excitation energy. The advantage of using two excitation lines is that we can distinguish in this complicated structure what is Raman and what is PL, since the PL must appear at a specific energy, while the Raman shift is referred to the laser line. Thus, in the lower plot we can observe the 4LO, 5LO and 6LO emission, while in the upper plot obtained with a higher excitation energy, we can see the 6LO, 7LO and 8LO. On the other hand, starting from lower energy we observe the PL due to the yellow band, the donor-acceptor pairs (DAP) around 2.3 eV and going to upper energy several exciton emissions coming from the 1s and 2s states of the light and heavy excitons of ZnTe. In Ref [16], several lines of a Kr-Ar laser were used, giving us, in the different Raman spectra, multi-phonon peaks up to 10LO phonons. These multi-phonon emissions are typical of 12-16 polar materials and are due to the strong electron-phonon interaction, more intense than in 13-15 materials.

8 Summary

In summary, after a short theoretical introduction of resonant Raman scattering and the importance of Fröhlich electron-phonon interaction in polar materials, we show a set of experimental examples where some peculiarities of some materials are better described or only appear in a Raman experiment in resonance with an electronic transition.

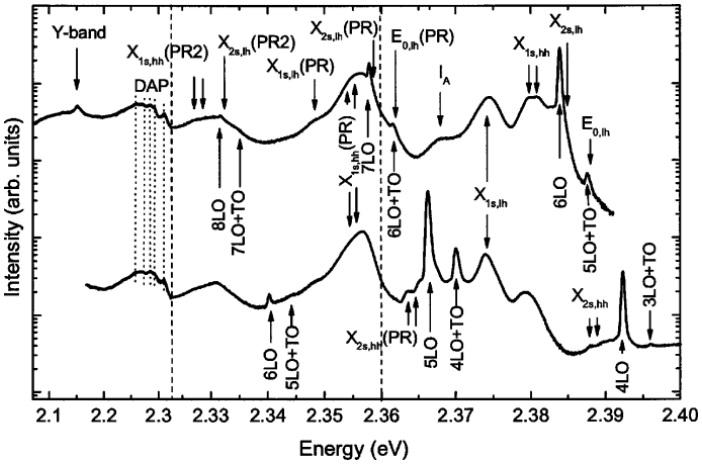

Fig 8. PL of the ZnTe/GaAs sample obtained with two excitation lines (see text) measured at 19 K. The figure is separated into three regions, marked with vertical dashed lines, the regions have different scale [16]. Reprinted with premission from AIP.

Funding Information

This work has been partially financed by grants RTI2018-093711-B-I00 and TED2021-129298B-I00, from the Ministry of Universities of Spain, and Prometeo2020-016 and from the Generalitat Valenciana.

References

1. Sood A K, Menéndez J, Cardona M, Ploog K, Resonance Raman Scattering by Confined LO and TO Phonons in GaAs-AlAs Superlattices, *Phys Rev Lett*, 54(1985)2111–2114.
2. (a) Comas F, Trallero-Giner C, Cantarero A, Optical Phonons and Electron-Phonon Interaction in Quantum Wires, *Phys Rev B*, 47(1993)7602–7605.

   (b) Comas F, Cantarero A, Trallero-Giner C., Moshinsky M, Polar Optical Oscillations in Quantum Wires and Free-Standing Wires: The Electron-Phonon Interaction Hamiltonian, *J Phys Condens Matter*, 7(1995)1789–1805.
3. Voutsas A T, Hatalis M K, Boyce J, Chiang A, Raman Spectroscopy of Amorphous and Microcrystalline Silicon Films Deposited by Low-pressure Chemical Vapor Deposition, *J Appl Phys*, 78(1995)6999–7006.
4. Cantarero A, Trallero-Giner C, Cardona M, Excitons in one-phonon resonant Raman scattering: Deformation-potential interaction, *Phys Rev B*, 39(1989)8388–8397.
5. Gontijo R N, Resende G C, Fantini C, Carvalho B R, Double Resonance Raman Scattering Process in 2D Materials, *J Mater Res*, 34(2019)1976–1992.
6. Alexandrou A, Trallero-Giner C, Cantarero A, Cardona M, Theoretical model of stress-induced triply resonant Raman scattering, *Phys Rev B*, 40(1989)1603–1610.
7. Tenne D A, Bruchhausen A, Lanzillotti-Kimura N D, Fainstein A, Katiyar R S, Cantarero A, Soukiassian A, Vaithyanathan V, Haeni J H, Tian W, Schlom D G, Choi K J, Kim D M, Eom C B, Sun H P, Pan X Q, Li Y L, Chen L Q, Jia Q X, Nakhmanson S M, Rabe K M, Xi X X, Probing Nanoscale Ferroelectricity by Ultraviolet Raman Spectroscopy, *Science*, 313(2006)1614–1616.

8. Capizzi M, Frova A, Optical Gap of Strontium Titanate (Deviation from Urbach Tail Behavior), *Phys Rev Lett*, 25(1970)1298–1302.
9. Suzuki K, Kijima K, Optical Band Gap of Barium Titanate Nanoparticles Prepared by RF-Plasma Chemical Vapor Deposition, *Jpn J Appl Phys*, 44(2005)2081–2082.
10. Teweldebrhan D, Goyal V, Balandin A, Exfoliation and Characterization of Bismuth Telluride Atomic Quintuples and Quasi-Two-Dimensional Crystals, *Nano Lett*, 10(2010)1209–1218.
11. Rodríguez-Fernández C, Manzano C V, Romero A H, Martín J, Martín-González M, de Lima M M (Jr), Cantarero A, The Fingerprint of Te-Rich and Stoichiometric Bi_2Te_3 Nanowires by Raman Spectroscopy, *Nanotech*, 27(2016)075706; doi.10.1088/0957-4484/27/7/075706.
12. Rodríguez-Fernández C, Almokhtar M, Ibarra-Henández W, Morais de Lima M, Romero AH, Asahi H, Cantarero A, Isotopic heft on the B_{11} silent mode in ultra-narrow gallium nitride nanowires, *Nano Lett*, 18(2018)5091–5097.
13. Ruf T, Serrano J, Cardona M, Pavone P, Pabst M, Krisch M, D'Astuto M, Suski T, Grzegory I, Leszczynski M, Phonon Dispersion Curves in Wurtzite-Structure GaN Determined by Inelastic X-Ray Scattering, *Phys Rev Lett*, 86(2001)906–909.
14. Kane C L, Mele E J, Z_2 topological order and the quantum spin hall effect, *Phys Rev Lett*, 95(2005)146802; doi.org/10.1103/PhysRevLett.95.146802.
15. Roddríguez-Fernández C, Akius K, de Lima M M, Cantarero A, van Ruitenbeek J M, Sabater C, Raman signal reveals the rhombohedral crystallographic structure in ultra-thin layers of bismuth thermally evaporated on amorphous substrate, *Mater Sci Eng B*, 270(2021)115240; doi.10.1016/j.mseb.2021.115240.
16. Camacho J, Cantarero A, Hernández-Calderón I, González L, Raman Spectroscopy and Photoluminescence of ZnTe Thin Films Grown on GaAs, *J Appl Phys*, 92(2002)6014–6015.

[*Received*: 22.02.2023; *accepted*: 28.02.2023]